

Research Paper

Cite this article: Jiang F (2023). SSA research on electromagnetic scattering in arid zone. *International Journal of Microwave and Wireless Technologies* **16**(1), 110–117. <https://doi.org/10.1017/S1759078723000247>

Received: 19 May 2022
Revised: 8 March 2023
Accepted: 8 March 2023

Keywords:

Arid zone; electromagnetic scattering characteristics; soil dielectric constant; SSA

Correspondence author:

Fengyun Jiang;
E-mail: fengyunjiang0930@126.com

Abstract

This paper investigates the electromagnetic scattering characteristics in arid zone and proposes methods for monitoring and improving ecological agriculture, vegetation landscape and desertification in arid zone, based on the modified small slope approximation (SSA) electromagnetic scattering model. The dielectric properties of dryland soils are studied in the paper, and the variation curves of soil dielectric constant with humidity and electromagnetic frequency are plotted. In order to reproduce the geomorphological features of the dryland areas, a two-dimensional geometric model of the ground environment is established using Monte Carlo methods combined with Gaussian spectral functions. An algorithm model based on the modified SSA is developed, and the algorithm was validated and analyzed to verify its reliability. In the simulations, the southeastern region of Ejina Banner, Inner Mongolia was taken as a typical arid region, and the simulation parameters are obtained from the actual measurement data of the region. The study finds that the electromagnetic scattering characteristics of the arid zone are influenced by soil water content, ground roughness and incident wave electromagnetic frequency, and there is regularity. The results of this paper can be effectively combined with remote sensing technology to contribute to many researches on soil moisture inversion and ecological condition of vegetation, which are important in many aspects such as irrigation control, ecological research, vorticity covariance, and climatology of slope stability.

Introduction

Arid areas are areas with dry climates, covering about 30% of the land area. Common features of arid areas are low precipitation, large temperature differences, evaporation may be much higher than precipitation, and water scarcity is the main factor limiting plant growth [1,2]. The frequent occurrence and long-term persistence of drought will not only bring huge losses to socio-economic, especially agricultural production, but also cause many adverse ecological and environmental impacts such as water shortage, increased desertification, and frequent sandstorms. At the same time, due to the abundance of heat, with reasonable irrigation and fertilization has the potential to become a high-yield area. For this reason, the study of arid areas, which focuses on various parameters such as water content, vegetation, sand and dust and temperature, can be studied and analyzed by radar remote sensing echoes [3–6] and scattering echoes [7–9] to obtain relevant information about arid areas. By extracting and analyzing useful data, it can contribute to many aspects such as environmental detection, breeding and grazing, target detection, and precision strikes.

It can be noted from literatures that international scholars have done a lot of research on the characteristics of environmental echoes under different environments, but relatively little research has been done on arid regions. Tian [10] calculated the snow electromagnetic scattering coefficients using the small perturbation method, and generalized the effects of moisture and roughness on snow scattering. The study of [10] is targeted and its findings are not applicable to other environmental facets. Comite [11] proposed a first-order small slope approximation (SSA) algorithm, established a reliable electromagnetic scattering model, studied the monostatic and bistatic scattering characteristics of cultivated land, and proposed a new understanding about anisotropic soil scattering, which is important for the inversion of soil water content. His study is very informative, but the effects of roughness and electromagnetic frequency are less studied. Johnson [12] established an approximate and accurate surface scattering model, focusing on the locations where the minima occur in the scattering of the two polarization modes HH and VV, and found that the locations vary with the polarization mode and the roughness. Han [13] focused on the soil types and compositions of saline, dry and wetlands, established a dielectric constant model, and proposed an inversion algorithm based on electromagnetic scattering. And the correctness of the inversion model was verified by case calculations. Han's research results can be used for soil moisture detection in saline soils, but its application is limited to some extent due to the specificity of its application.

In this paper, we focus on electromagnetic scattering in arid regions, and the experimental parameters are based on measured data from the southeastern region of Ejina Banner, Inner Mongolia [14]. Moreover, an accurate soil dielectric constant model is established and the effects of various factors, such as electromagnetic frequency and soil moisture, on the soil dielectric constant are summarized. In terms of research method, the traditional SSA method is modified in this paper to speed up the calculation process and reduce the error, and the correctness of the modified SSA is verified by simulation. Finally, it is found that the scattered echoes in arid areas have a large relationship with electromagnetic wave band, soil water content and ground roughness, and this connection is linear and regular.

Four component soil dielectric model

Soil dielectric constants are affected by various factors, and an accurate mathematical model to describe the dielectric properties of soils is necessary if highly accurate soil-related information is to be obtained. In this subsection, a four-component dielectric model for soils in arid regions was developed, and the effects of water content and electromagnetic band on the dielectric constant of soils were investigated. According to the four-component soil dielectric model, the empirical equations are as follows [15]

$$W_p = 0.06774 - 0.00064S + 0.00478C \quad (1)$$

$$m_t = 0.49W_p + 0.165 \quad (2)$$

In the above formula, W_p stands for soil moisture compression point, m_t stands for critical body moisture. $S(\%)$ represents the sand content of the soil and $C(\%)$ represents the clay content. The dry soil density is represented by the symbol ρ_b :

$$\rho_b = 3.455 / (25.1 - 0.0021S + 0.0022C)^{0.3018} \quad (3)$$

$$p = 1 - \frac{\rho_b}{\rho_s} \quad (4)$$

where ρ is the pore accumulation rate of the soil, ρ_s represents the density of the rock in the soil and generally takes the value 2.65 g/cm^3 .

Soil moisture is represented by the symbol m_v and is often used to calculate the relative dielectric constant of the soil.

$$\varepsilon = m_v \varepsilon_x + (p - m_v) \varepsilon_a + (1 - p) \varepsilon_r \quad (m_v \leq m_t) \quad (5)$$

$$\varepsilon = m_t \varepsilon_x + (m_v - m_t) \varepsilon_w + (p - m_v) \varepsilon_a + (1 - p) \varepsilon_r \quad (m_v > m_t) \quad (6)$$

$$\varepsilon_x = \varepsilon_i + (\varepsilon_w - \varepsilon_i)(-0.57W_p + 0.481) \quad (7)$$

In the above equation, the relative permittivity of ice, rock and air are represented by ε_i , ε_r and ε_a , respectively, whose values can be found in the literature [14]. The relative permittivity of pure water is

$$\varepsilon_w = \varepsilon_{w\infty} + \frac{\varepsilon_{w0} - \varepsilon_{w\infty}}{1 + j2\pi f \tau_w} \quad (8)$$

In the above Debye equation, ε_{w0} denotes DC permittivity, τ_w denotes relaxation time, and $T(^{\circ}\text{C})$ denotes soil temperature. They are related as

$$2\pi\tau_w = 1.1109 \times 10^{-10} - 3.824 \times 10^{-12}T + 6.938 \times 10^{-14}T^2 - 5.096 \times 10^{-16}T^3 \quad (9)$$

$$\varepsilon_{w0} = 88.045 - 0.4147T + 6.295 \times 10^{-4}T^2 + 1.075 \times 10^{-5}T^3 \quad (10)$$

The effects of soil moisture and electromagnetic wave frequency on the relative permittivity were plotted in Fig. 1.

Rough surface modeling and scattering calculation

Two-dimensional rough surface modeling

In the study of this paper, in order to improve the accuracy of the model, the two-dimensional rough surface was generated with full consideration of the actual conditions of the soil ground and integrating the Monte Carlo method [16] and the Gaussian spectral function [17].

The surface height function of a two-dimensional rough surface is

$$f(x, y) = \frac{1}{L_x L_y} \sum_{m=-\infty}^{\infty} \sum_{n=-\infty}^{\infty} b_{mn} \exp\left(\frac{j2\pi mx}{L_x}\right) \exp\left(\frac{j2\pi ny}{L_y}\right) \quad (11)$$

In the formula, L_x , L_y represents the length of the rough surface in two dimensions, and $b_{m,n}$ is calculated as

$$b_{mn} = 2\pi \sqrt{L_x L_y W(k_{xm}, k_{yn})} \cdot \alpha \quad (12)$$

$$\alpha = \begin{cases} \frac{N(0, 1) + jN(0, 1)}{\sqrt{2}} & m \neq 0, N_x/2, n \neq 0, N_y/2 \\ N(0, 1) & m = 0, N_x/2 \text{ or } n = 0, N_y/2 \end{cases} \quad (13)$$

$N(0, 1)$ is the random sampling points on the normal distribution, N_x and N_y are the number of sampling points on the rough surface in two dimensions, $W(k_{xm}, k_{yn})$ represents

$$W(k_{xm}, k_{ym}) = \frac{l_x l_y h^2}{4\pi} \exp\left(-\frac{k_x^2 l_x^2}{4} - \frac{k_y^2 l_y^2}{4}\right) \quad (14)$$

where h is the root-mean-square height of the Gaussian rough surface, l_x and l_y are the correlation lengths of the rough surface in two dimensions, k_{xm} and k_{yn} are the discrete points of the spatial frequencies in two dimensions, respectively.

$$k_{xm} = \frac{2\pi m}{L_x}, \quad k_{yn} = \frac{2\pi n}{L_y} \quad (15)$$

The schematic diagram of the two-dimensional rough surfaces with different roughness generated by the method in this paper is shown in Fig. 2.

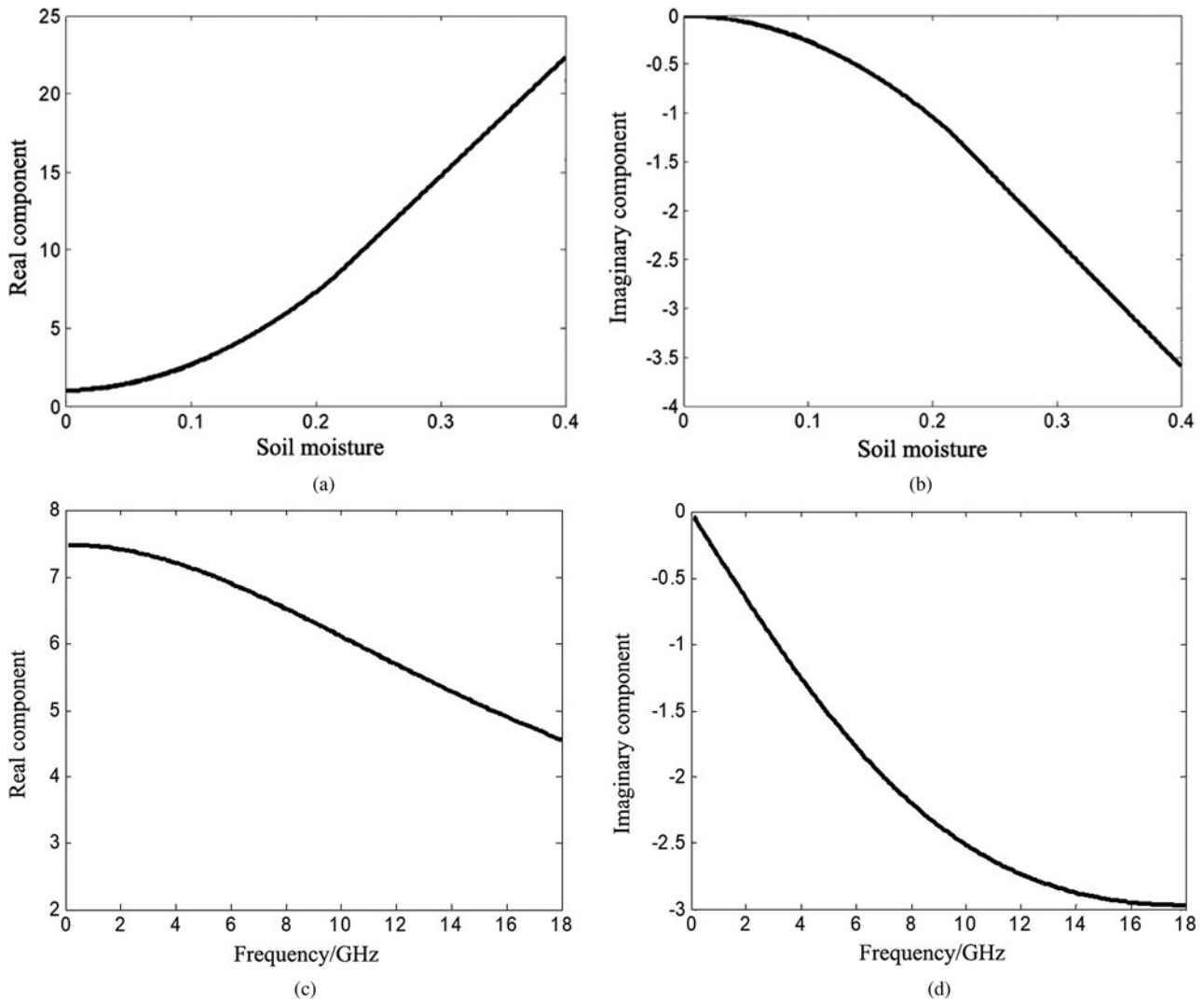


Figure 1. Soil dielectric constant curve. (a) Real component - soil moisture; (b) Imaginary part - soil moisture; (c) Real part - electromagnetic frequency; (d) Imaginary part - electromagnetic frequency.

Conical incident wave

A finite truncation of the infinitely extended rough surface is required in the numerical calculation. In order to eliminate the effects such as reflection and edge bypassing caused by the abrupt truncation of the rough surface edge, a conical incident wave is used instead of plane wave incidence.

The conical wave requires attention to the beam width, which determines the irradiation width of the incident wave. When it is too large, the size of the rough surface needs to be increased accordingly to ensure the irradiated area; when it is too small, the rough surface and the target cannot be fully irradiated and a reasonable compound scattering field cannot be obtained. Reasonable calculation results and faster efficiency can be obtained when g and rough surface size L satisfy the following relationship

$$g \geq \frac{6}{(\cos \theta_i)^{1.5}}, L = 4g \quad (16)$$

For TE incident waves, the incident electromagnetic field is

$$E_{inc}(\mathbf{r}) = \int_{-\infty}^{+\infty} \int_{-\infty}^{+\infty} \exp(jk_x x + jk_y y - jk_z z) \cdot E(k_x, k_y) \mathbf{h}_i(-k_z) dk_x dk_y \quad (17)$$

$$\mathbf{H}_{inc}(\mathbf{r}) = -\frac{1}{\eta_0} \int_{-\infty}^{+\infty} \int_{-\infty}^{+\infty} \exp(jk_x x + jk_y y - jk_z z) \cdot E(k_x, k_y) \mathbf{v}_i(-k_z) dk_x dk_y \quad (18)$$

where $E(k_x, k_y)$ is the incident spectrum, and the horizontal polarization direction \mathbf{h}_i and vertical polarization direction \mathbf{v}_i are denoted as

$$\mathbf{h}_i(-k_z) = \frac{1}{k_p} (xk_y - yk_x) \quad (19)$$

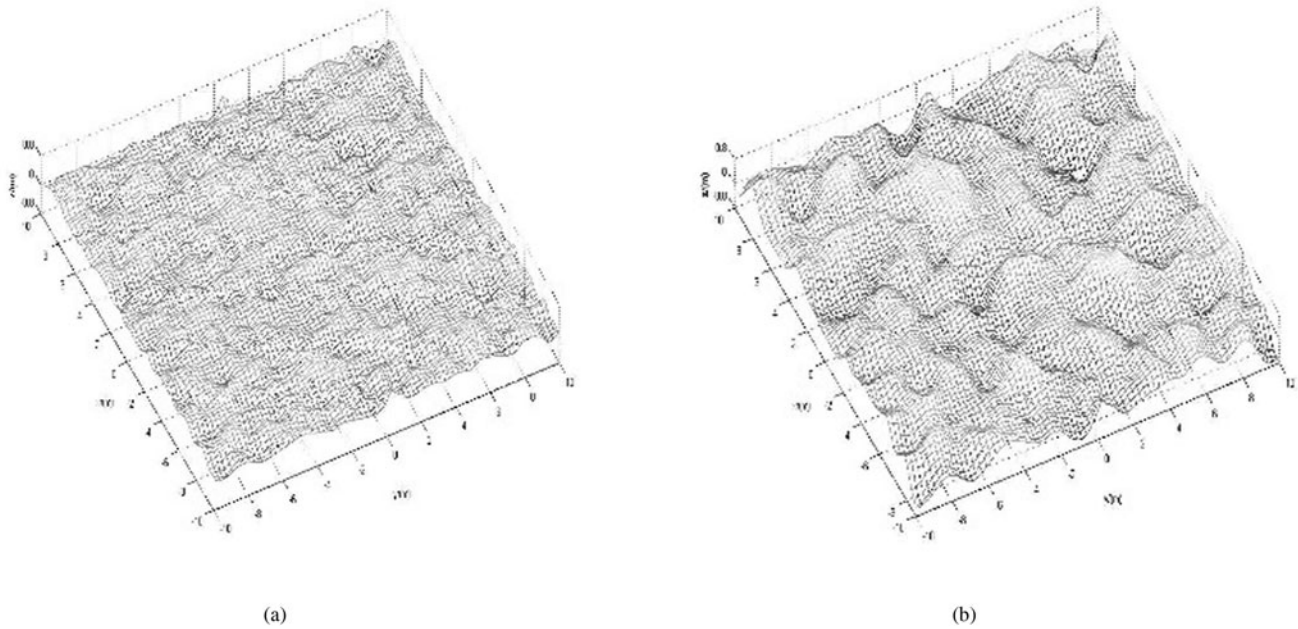


Figure 2. Rough surface model. (a) $h = 0.1$ m, $l_x = l_y = 0.5$ m; (b) $h = 0.3$ m, $l_x = l_y = 1.0$ m.

$$\mathbf{v}_i(-k_z) = \frac{k_z}{k_0 k_\rho} (\mathbf{x} k_x + \mathbf{y} k_y) + \frac{k_\rho}{k_0} \mathbf{z} \quad (20)$$

η_0 is the free space wave impedance, k_x, k_y, k_z are the spatial spectral domains in the x, y, z directions, respectively, $k_\rho = \sqrt{k_x^2 + k_y^2}$. For TM incident waves, the incident electromagnetic field is

$$\mathbf{E}_{inc}(\mathbf{r}) = \int_{-\infty}^{+\infty} \int_{-\infty}^{+\infty} \exp(jk_x x + jk_y y - jk_z z) \cdot E(k_x, k_y) \mathbf{v}_i(-k_z) dk_x dk_y \quad (21)$$

$$\mathbf{H}_{inc}(\mathbf{r}) = -\frac{1}{\eta_0} \int_{-\infty}^{+\infty} \int_{-\infty}^{+\infty} \exp(jk_x x + jk_y y - jk_z z) \cdot E(k_x, k_y) \mathbf{h}_i(-k_z) dk_x dk_y \quad (22)$$

The angles of the incident waves are set to $\theta_i = 60^\circ, \varphi_i = 0^\circ$, and the two-dimensional normalized conical incident wave amplitudes are shown in Fig. 3. From the figure, it can be seen that the magnetic field is strongest at the center of the rough surface, and the farther away from the center, the weaker the magnetic field is, which slowly goes to zero at the edge. Therefore, the errors caused by the truncation of the rough surface can be avoided in the numerical simulation.

Modified small slope approximation

Based on the fact that the soil rough surface is anisotropic, the classical SSA method with appropriate modifications is used in this paper.

The core of the SSA method to solve the electromagnetic scattering problem is to solve for the scattering amplitude T . In the scattering field calculation, the solution equation for T is as follows

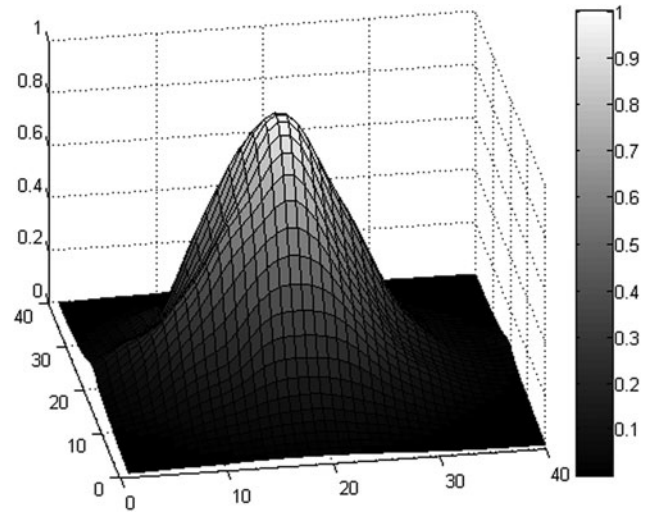


Figure 3. Normalized conical wave schematic.

$$T(\mathbf{q}, \mathbf{k}) = - \int_S e^{-i\mathbf{q} \cdot \mathbf{x}} \hat{\mathbf{n}} \cdot \nabla P_k(\mathbf{x}) dS \quad (23)$$

where the point on the scattering cross section S is labeled by the two-dimensional vector \mathbf{x} , $P_k(\mathbf{r})$ satisfying the boundary conditions and the Helmholtz equation.

$$(\nabla^2 + k^2)P_k(\mathbf{r}) = 0 \quad (24)$$

Its complete solution can be obtained by integrating:

$$P_k(\mathbf{r}) = e^{i\mathbf{k} \cdot \mathbf{r}} - \frac{1}{4\pi} \int_S G_k(\mathbf{r} - \mathbf{x}) \hat{\mathbf{n}} \cdot \nabla P_k(\mathbf{x}) dS \quad (25)$$

$$G_k(\mathbf{r} - \mathbf{x}) = e^{ik|\mathbf{r} - \mathbf{x}|}/|\mathbf{r} - \mathbf{x}| \quad (26)$$

where \mathbf{r} is the surface element vector and $G_k(\mathbf{r} - \mathbf{x})$ represents the Green's function.

According to the above equation, the scattering amplitude value T of the soil rough surface can be found, which in turn leads to σ_{suf} :

$$\sigma_{suf} = \langle T^* T \rangle / 16\pi^2 \quad (27)$$

Combine (23)(24) (25)(26)(27):

$$\sigma_{suf} = \frac{2}{\pi} \left(\frac{k_z q_z}{Q_h Q_z} \right)^2 \cdot I(\alpha) \quad (28)$$

$$\alpha = \frac{0.08\pi}{200[\Gamma(7/4)^2]} \left[\left(\frac{u^2}{g} \right)^{1/2} \frac{Q_z^2}{Q_h^{3/2}} \right] \quad (29)$$

$I(\alpha)$ is the spectral integral of the rough surface and $\mathbf{k} - \mathbf{q} = (Q_h, Q_z)$. Q_h and Q_z can be solved by the following equations.

$$Q_h = k_0 \cdot \sqrt{\cos^2 \theta_{inc} + \cos^2 \theta_{scat} - 2 \cos \theta_{inc} \cos \theta_{scat} \cos \phi_{bi}} \quad (30)$$

$$Q_z = -k_0(\sin \theta_{inc} + \sin \theta_{scat}) \quad (31)$$

It can be found that the soil rough surface scattering coefficient depends on the following integral.

$$I(\alpha) = \int_0^\infty J_0(y) y B(y, \alpha) dy \quad (32)$$

where

$$J_0(y) = \sum_{n=0}^\infty \frac{(-y^2/4)^n}{(n!)^2} \quad (33)$$

$$B(y, \alpha) = \exp(-\alpha y^{1.5}) \quad (34)$$

In the above equation, $J_0(y)$ is the first class zero-order Bessel function and $B(y, \alpha)$ is the calculated coefficient.

Combining the above equations, $I(\alpha)$ can be expanded into the following equation:

$$I(\alpha) = \frac{2}{3} \alpha^{-4/3} \sum_{n=0}^\infty \frac{(-n)^n}{(n!)^2} \cdot \left(\frac{1}{4\alpha^{4/3}} \right)^n \Gamma\left(\frac{4(n+1)}{3}\right) \quad (35)$$

The summation based on the traditional SSA requires manual truncation, and when α is large, the formula converges quickly and the error generated by manual truncation is small; when α is small, the formula converges slowly, which will lead to the error generated by truncation beyond the engineering range, which is uncontrollable in the actual calculation, so it is unrealistic to apply equation (35) for the solution. Therefore, modifications based on the traditional SSA method can be considered to speed up the calculation process and reduce the error.

Based on the above idea, we can find that $\Gamma(-z)$ has a remainder $-(-1)^n/n!$ at a non-negative integer n . Obviously, by applying the residue theorem, the series terms in $I(\alpha)$ can be turned into:

$$\begin{aligned} & \sum_{n=0}^\infty \frac{(-n)^n}{(n!)^2} \cdot \frac{1}{4\alpha^{4/3}} \Gamma\left(\frac{4(n+1)}{3}\right) \\ &= -\frac{1}{2\pi i} \int_C \frac{\Gamma(-z) \Gamma\left[\frac{4(n+1)}{3}\right]}{\Gamma(z+1)} \left(\frac{1}{4\alpha^{4/3}}\right)^z dz \end{aligned} \quad (36)$$

Substituting (36) back into (35):

$$\begin{aligned} I(\alpha) &= -\frac{2}{\pi} \sum_{n=0}^N \frac{(-\alpha)^n}{(n!)^2} \cdot \left[\Gamma\left(\frac{4}{3}n+1\right) \right]^2 \cdot \sin \frac{3\pi n}{4} 2^{3n/2} \\ &\quad \pm R_N \end{aligned} \quad (37)$$

where

$$R_N = \alpha^{N+0.5} A(N) B(N) \quad (38)$$

$$A(N) = [2^{4.25+1.5N} e^{-1/2(N+2.5)} 0.75^{N+1} \cdot x^{0.5(N+3.5)}] / 3\sqrt{\pi} \quad (39)$$

$$\begin{aligned} B(N) &= \int_0^\infty (1+u^2)^{\frac{1}{3}(3N+3.5)} \left[\left(1 + \frac{1}{4x}\right)^2 + u^2 \right]^{-(N+1)/2} \\ &\quad \exp \left[-xu \left(2 \tan^{-1} u - \frac{4}{3} \tan^{-1} \frac{u}{1-1/x} \right) \right] \cdot \frac{\cosh(\pi x u)}{\cosh(4\pi x u/3)} du \end{aligned} \quad (40)$$

In the above equation, $B(N)$ decays exponentially, and the decay accelerates as u increases.

Thus, the modified SSA method can be used to calculate the scattering coefficient of soil rough surface to ensure the accuracy and calculation speed at the same time, which meets the engineering requirements.

Validation of algorithm

The main work of this subsection is to verify the correctness of the SSA algorithm used in this paper. The validation algorithm uses the MOM algorithm, which is convincingly accurate and precise in its calculation. In the validation, both SSA and MOM methods were used to calculate the backscattering coefficients for the same rough surface with the following settings of the rough surface parameters with reference to the arid region: dimension $L_x \times L_y = 10\lambda \times 10\lambda$, correlation length $l_x \times l_y = 0.8\lambda \times 0.8\lambda$, root mean square height $h = 0.1\lambda$, dielectric constant (13.61, -0.03) and incident wave frequency $f = 300\text{MHz}$.

The calculation results of the two methods are plotted in Fig. 4, and the two curves match well, indicating that the algorithm is effective in calculating the rough surface of Gaussian media.

Calculation results and analysis

The soil data in this paper were obtained from the measured data in the southeastern part of Ejina Banner, Inner Mongolia, which

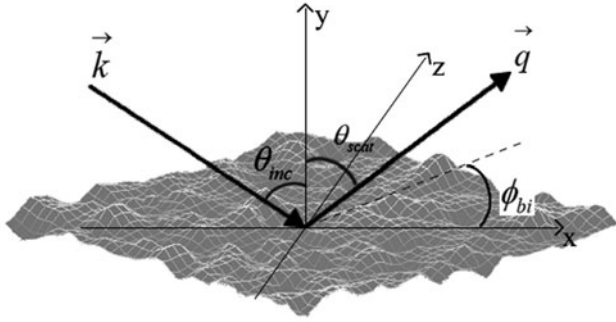


Figure 4. Electromagnetic Scattering Model.

has typical characteristics of an arid region with little rainfall, high evaporation, sufficient sunshine, large temperature difference and sandy wind. The soil of this arid land is mainly composed of sand, chalk and clay, accounting for 66.97%, 20.78 and 12.25%, respectively, with a density of 1.173 g/cm³ and an average water content of 10.35%.

In the simulation, the effects of different soil roughness, different soil moisture content and different incident wavelengths on the backscattering characteristics in arid regions are mainly studied and discussed. Where, the size of the rough surface is $L_x \times L_y = 10\lambda \times 10\lambda$, and the correlation length is $l_x \times l_y = 0.8\lambda \times 0.8\lambda$.

Influence of different roughness

This subsection focuses on the effects of different soil roughness on the scattering characteristics in arid regions, and the backscattering coefficients were calculated for root-mean-square heights of 0.05, 0.10 and 0.15 m, respectively, and plotted in Fig. 5. The incident wave frequency is 300 MHz, the soil moisture content is 10.35%, and the HH and VV polarization results are as follows.

Observing Fig. 6, in general, the scattering intensity decreases linearly with the increase of radar incidence angle, and the scattering intensity is maximum when the incident wave is perpendicular to the ground. From the calculation results of different roughness, as the soil roughness becomes larger, the backward scattering increases, and they are positively correlated. According to this property, the roughness of the region can be obtained by comparison. And the roughness of arid areas is often affected by desertification - the more severe the

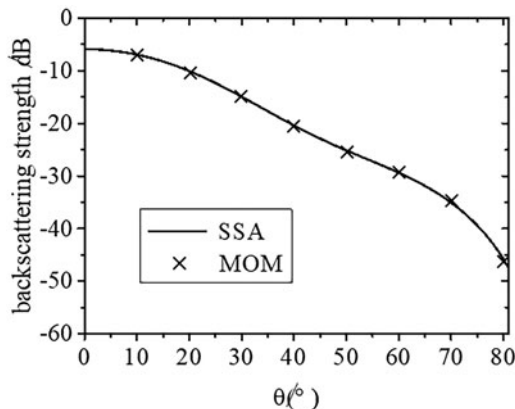


Figure 5. Validation of Algorithm.

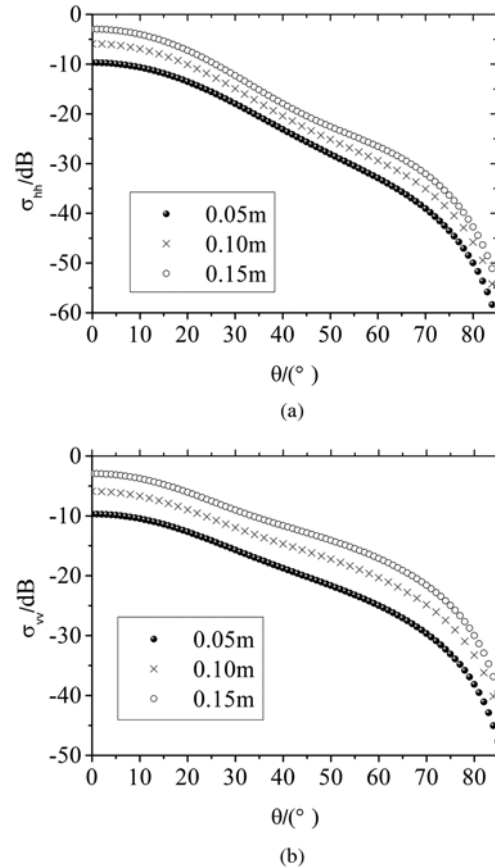


Figure 6. Curves with different root mean square. (a) HH polarization; (b) VV polarization.

desertification, the more sand and gravel fill the gullies, the flatter the land surface, the lower the roughness, so to some extent it can reflect the degree of desertification in the area. In another way, the intensity of the backscattering coefficient in a certain area can be continuously detected to study whether the desertification in the area has been aggravated or weakened, and to provide a reference for the subsequent decision of regional management.

Effect of soil moisture content

In arid areas where precipitation is scarce and evaporation is high, water scarcity is a major limiting factor for plant growth. However, arid areas have enough heat and they have the potential to become highly productive if they receive proper irrigation and fertilization. Therefore, this subsection calculates the scattering coefficients of soils with different moisture levels and discusses their scattering characteristics.

According to the actual measurement data in the southeastern part of Ejina Banner, Inner Mongolia, the soil moisture content varies greatly in different periods, with the highest value of 38.07% and the lowest value of 0.23%. In order to fully investigate the electromagnetic scattering characteristics in arid regions, the scattering results were calculated for two extreme water content conditions, as shown in Fig. 7.

It was found that for the HH polarization results, the two curves could be clearly distinguished in the (0°, 85°) range, and their overlap was very small. While in the VV polarization mode, the scattering coefficients of soils with different moisture contents become

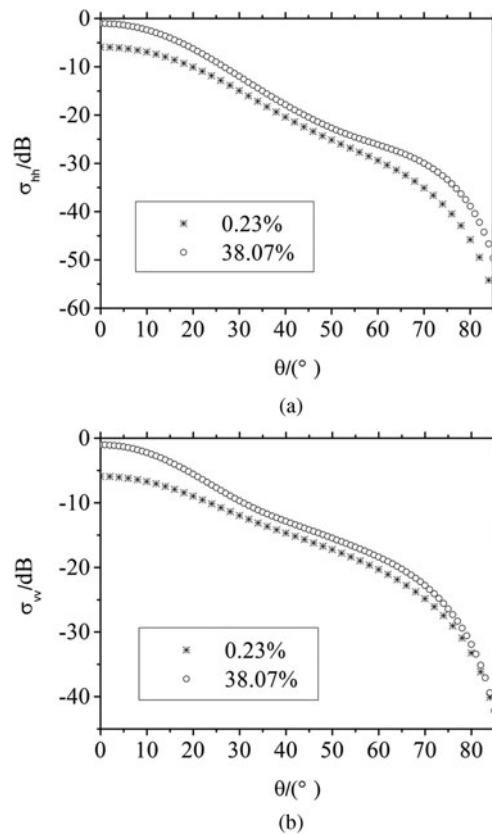


Figure 7. Curves with different soil moisture content. (a) HH polarization; (b) VV polarization.

closer and closer with increasing angles, and finally almost overlap. In general, the soil moisture content has a strong influence on the scattering coefficients, and the differences are greatest when the incident wave is perpendicular to a rough surface, which can be easily distinguished with the naked eye. It can be inferred from the simulated results of soil water content under two extreme conditions in the region that soil water content is an important factor affecting the electromagnetic scattering characteristics in arid regions. The variation of soil water content will lead to fluctuations of electromagnetic scattering intensity on the rough surface. The results of this paper can be combined with remote sensing techniques to invert soil water content based on radar scattering coefficients, which is important for soil water content studies such as

irrigation control, ecological studies, vorticity covariance, and slope stabilization climate science.

The frequency effect

Different wavelengths of electromagnetic waves have different penetrating abilities and different sensitivities to rough surface parameters. Therefore, it is important to study the electromagnetic scattering characteristics of arid areas under different electromagnetic spectrum environments and find the electromagnetic “optimal solution” for environmental protection and ecological monitoring.

In this subsection of the study, the soil moisture content was 10.35% and the root mean square height of the rough surface was 0.05 m. The calculated results were plotted in Fig. 8.

Through the curves we can find that, intuitively, the backscattering coefficient of the arid rough surface decreases continuously with the increase of the incident wave electromagnetic frequency. However, there are some differences between the results of HH polarization and VV polarization: ①For the VV polarization results, in the range of (0°, 90°), the three curves always do not intersect and are distinguished obviously; ②For the HH polarization results, in the angle of (0°, 48°), the three curves can be distinguished by the naked eye; in the range of (49°, 90°), the scattering coefficients of the three frequencies are extremely close to each other, and the magnitude cannot be determined by visual observation.

Therefore, when studying the effect of electromagnetic frequency on the scattering coefficient, better results can be obtained by choosing the incident wave with VV polarization.

Calculation

This paper focuses on the electromagnetic scattering characteristics in arid regions, and the parameters in the study are all derived from the measured data in the southeast of Ejinaqi, Inner Mongolia [14]. Soil water content, ground roughness and incident wave frequency were found to be important influencing factors in the study, and the scattering coefficients in arid lands subsequently showed regular variations. The reasons for the appearance of this regular characteristic were analyzed, and improved methods for monitoring soil moisture and desertification control were proposed, which have important significance in agricultural and ecological management. Besides, the results of this paper can be effectively combined with remote sensing technology to invert soil water content and study the

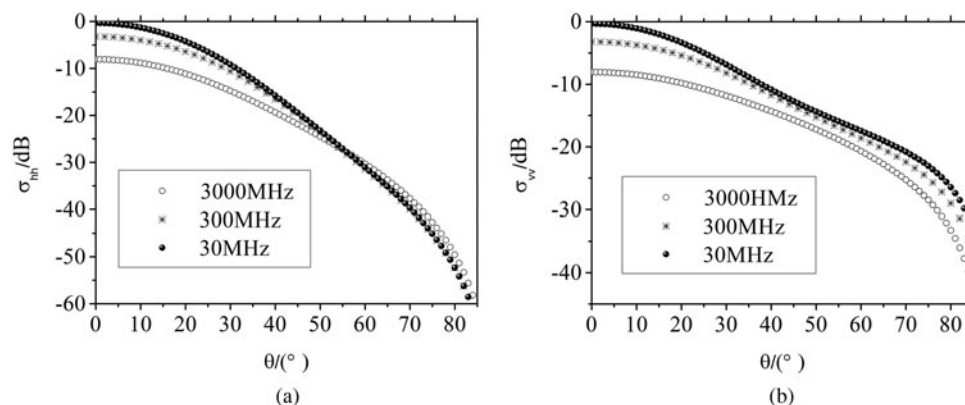


Figure 8. Curves with different frequencies. (a) HH polarization; (b) VV polarization.

ecological situation of vegetation, which is important for soil water content studies, such as irrigation control, ecological studies, vorticity covariance, slope stability climatology, etc. In the next research, it is planned to apply remote sensing technology to promote multi-faceted research on geomorphology, climate, and vegetation in arid regions.

Conflict of interest. There are no conflicts of interest to disclose for all the authors.

References

1. Guo QQ, Qu JJ, Wang GH, Xiao JH and Pang YJ (2015) Progress of wetland researches in arid and semi-arid regions in China. *Arid Zone Research* **32**, 213–220.
2. Guan XD, Cheng SJ, Guo RX and Ji MX (2014) Review of researches on numerical simulation of soil moisture over the arid and semi-arid region. *Journal of Arid Meteorology* **32**, 135–141.
3. Khanal S, Klopfenstein A, Kushal KC, Ramarao V, Fulton J, Douridas N and Shearer SA (2021) Assessing the impact of agricultural field traffic on corn grain yield using remote sensing and machine learning. *Soil & Tillage Research* **208**, 104880.
4. Zhao XW, Pan S, Sun ZC, Guo HD, Zhang L and Feng K (2021) Advances of satellite remote sensing technology in earthquake prediction. *Natural Hazards Review* **22**, 03120001.
5. Nhamo L, Ebrahim GY, Mabhaudhi T, Mpandeli S, Magombeyi M, Chitakira M, Magidi J and Sibanda M (2019) An assessment of groundwater use in irrigated agriculture using multi-spectral remote sensing. *Physics and Chemistry of the Earth* **115**, 102810.
6. Sarala D and Jacob S (2014) Digital image processing – a remote sensing perspective. *International Journal of Innovative Research and Development* **3**, 295–300.
7. Li JX, Zhang M, Jiang WQ and Wei PB (2020) Improved FBAM and GO/PO method for EM scattering analyses of ship targets in a marine environment. *Sensors (Basel, Switzerland)* **20**, 4735.
8. Ross G (2010) Electromagnetic scattering and its applications. *Optica Acta: International Journal of Optics* **29**, 725.
9. Rowell RL and Stein RS (1965) Electromagnetic scattering. *Science (New York, N.Y.)* **149**, 1399.
10. Tian AM (2019) Simulation Method of EM Scattering from Layered Rough Surface and Its Application in Snow. *Xidian University*.
11. Comite D and Pierdicca N (2019) Monostatic and bistatic scattering modeling of the anisotropic rough soil. *IEEE Transactions on Geoscience and Remote Sensing* **57**, 2543–2556.
12. Johnson JT and Ouellette JD (2014) Polarization features in bistatic scattering from rough surfaces. *IEEE Transactions on Geoscience and Remote Sensing* **52**, 1616–1626.
13. Han GH (2013) Soil Surface Moisture Inversion Research on Salt-Affected Soils by Polarimetric Radar in Arid Areas. *Xingjiang University*.
14. Xie W (2019) Inversion of Soil Moisture in Arid Area Based on C- and L-Band SAR Images. *Chang'an University*.
15. Wang R, Guo LX and Wang AQ (2010) Investigation of electromagnetic scattering interaction between the buried target and the rough surface in different types of soil. *Acta Physica Sinica* **59**, 3179–3186.
16. Caflisch RE (1998) Monte Carlo and quasi-Monte Carlo methods. *Acta Numerica* **7**, 1–49.
17. Bourlier C, Bergine G and Saillard J (2001) Theoretical study on two-dimensional Gaussian rough sea surface emission and reflection in the infrared frequencies with shadowing effect. *IEEE Transactions on Geoscience and Remote Sensing* **39**, 379–392.



Fengyun Jiang was born in Jiangxi, China. She received the bachelor and master degree from Hohai University and Nanchang University, in 1999 and 2007, respectively. She is currently a lecturer of Yichun University, Yichun, Jiangxi, China. Her research interests include electromagnetic computing.